

Synthesis, characterization and nonisothermal decomposition kinetics of $\text{La}_2(\text{CO}_3)_3 \cdot 3.4\text{H}_2\text{O}$

Xiang-hui Zhang · Chuan He · Ling Wang ·
Zhong-quan Li · Qian Feng

Received: 24 June 2014 / Accepted: 3 January 2015 / Published online: 30 January 2015
© Akadémiai Kiadó, Budapest, Hungary 2015

Abstract The single-phase $\text{La}_2(\text{CO}_3)_3 \cdot 3.4\text{H}_2\text{O}$ with the orthorhombic type was synthesized by hydrothermal method. The results characterized by XRD, FTIR and DTA–TG showed that the thermal decompositions of $\text{La}_2(\text{CO}_3)_3 \cdot 3.4\text{H}_2\text{O}$ below 1,273 K experience four steps, which involve a two-stage dehydration and formation of anhydrous $\text{La}_2(\text{CO}_3)_3$ at first, and then the formation of $\text{La}_2\text{O}_2\text{CO}_3$ and La_2O_3 , respectively. An additional intermediate product assigned to $\text{La}_2\text{O}(\text{CO}_3)_2$ was observed in the third step. Thermal decomposition kinetics of $\text{La}_2(\text{CO}_3)_3$ to $\text{La}_2\text{O}_2\text{CO}_3$ was investigated under nonisothermal conditions. The dependence of the activation energy on the

reaction degree was estimated by Ozawa and Friedman isoconversional methods, which confirm that the step is a multistage kinetic process. The reaction mechanism determined by a multivariate nonlinear regression program is a kind of two-stage consecutive reaction (A_n – A_n model), $f(x) = n(\ln(1 - \alpha^{(1 - 1/n)})(1 - \alpha))$. The first stage: $E = 435 \pm 9 \text{ kJ mol}^{-1}$, $\lg A = 28.7 \pm 0.8$, $\text{Dimension}1 = 0.28$; the second stage: $E = 234 \pm 4 \text{ kJ mol}^{-1}$, $\lg A = 13.5 \pm 0.3$, $\text{Dimension}2 = 1.22$.

Keywords Nonisothermal kinetics · Lanthanum carbonate hydrates · Thermal decomposition mechanism · Intermediate products

X. Zhang (✉) · L. Wang (✉)
College of Materials and Chemistry and Chemical Engineering,
Chengdu University of Technology, Chengdu 610059,
People's Republic of China
e-mail: zhangxianghui@cdut.cn; zhxh@cdut.edu.cn

L. Wang
e-mail: wangling@cdut.edu.cn

C. He
College of Mechanical and Electrical Engineering, Central South
University, Changsha 410012, People's Republic of China

Z. Li
State Key Laboratory of Oil and Gas Reservoir Geology and
Exploitation, Chengdu University of Technology,
Chengdu 610059, People's Republic of China

Z. Li
Key Laboratory of Tectonic Controls on Mineralization and
Hydrocarbon Accumulation, Ministry of Land and Resources,
Chengdu University of Technology, Chengdu 610059,
People's Republic of China

Q. Feng
NETZSCH Scientific Instrument Trading Co., LTD, Chengdu
Branch, Chengdu 610015, People's Republic of China

Introduction

Now as an effective, safe and ideal oral phosphate binder, hydrated lanthanum carbonates ($\text{La}_2(\text{CO}_3)_3 \cdot x\text{H}_2\text{O}$, $x = 1$ –10) especially with about 3–4 molecules of crystal water have been used to treat hyperphosphatemia in patients with renal failure [1, 2]. Additionally, as an industrial raw material, hydrated lanthanum carbonates can be used to the preparation of lanthanum oxide (La_2O_3) through thermal decomposition. La_2O_3 has also wide-ranging industrial and technological applications in several fields such as exhaust gas converters [3], catalyst of oxidative coupling of methane [4], arc electrode materials [5], a refractory oxide for optical glass [6] and other functional materials. However, these applications are mainly governed by the calcination process and purify of as-prepared hydrated lanthanum carbonates [7].

Date to several works has been focused on synthesis of the lanthanum carbonate hydrates with different molecules

of crystal water [1, 8–10]. The thermal decomposition of hydrated lanthanum carbonates has also been investigated extensively by many authors using SEM, XRD, FTIR and thermal analysis techniques [1, 8–10]. These works showed that more intermediate products were involved besides those reported $\text{La}_2(\text{CO}_3)_3 \cdot x\text{H}_2\text{O}$, $\text{La}_2(\text{CO}_3)_3$, $\text{La}_2\text{O}_2(\text{CO}_3)$ and La_2O_3 . The formation of lanthanum dioxycarbonate, $\text{La}_2\text{O}_2\text{CO}_3$, was also published as a similar feature in the decomposition of hydrated lanthanum carbonates. The thermal decomposition of anhydrous $\text{La}_2(\text{CO}_3)_3$ to $\text{La}_2\text{O}_2\text{CO}_3$ is often reported to occur in a single step by using conventional thermal analysis techniques [7, 8, 10]. However, an additional intermediate stage assigned to the formation of $\text{La}_2\text{O}(\text{CO}_3)_2$ had also been observed by using unconventional HT-DRIFT and HT-XRD techniques in the decomposition mentioned above and occurred in the following two-stage mechanisms: $\text{La}_2(\text{CO}_3)_3 (\text{s}) \rightarrow \text{La}_2\text{O}(\text{CO}_3)_2 (\text{s}) + \text{CO}_2 (\text{g})$ (1); $\text{La}_2\text{O}(\text{CO}_3)_2 (\text{s}) \rightarrow \text{La}_2\text{O}_2\text{CO}_3 (\text{s}) + \text{CO}_2 (\text{g})$ (2) [11, 12]. In addition, La_2O_3 obtained by thermal decomposition of the above-mentioned intermediate $\text{La}_2\text{O}_2\text{CO}_3$ above 873 K had also been reported extensively as a frequently feature [7–10]. Due to the formation of intermediate $\text{La}_2\text{O}_2\text{CO}_3$ is a complex process [11, 12], some reaction features such as conversion path, solid-state reactants, the reaction degree and activation energy will directly affect the structure and performances of the final product. To improve the product quality of lanthanum carbonate hydrates and La_2O_3 , it is very important to clarify the decomposition mechanism of $\text{La}_2(\text{CO}_3)_3$ to $\text{La}_2\text{O}_2\text{CO}_3$ based on conventional thermal analysis. The study of the decomposition kinetics can help to understand the complexity of the formation of oxide structured materials [13]. The investigation of conversion mechanism allows not only the quantitative precipitation of cations in solution, but also the control of some physicochemical properties of the resulting oxide via the thermal treatment (morphology, surface area, impurities, etc.) [14]. The investigation results of the kinetics and mechanism can provide valuable information on the optimum conditions in industrial production, such as the kinetic parameter for the accurate design of the installations and the treatment conditions, because augmentation of temperature or elongation of reaction time means more cost [15]. Due to it is not clear at present and needs further investigation.

In this study, the single-phase lanthanum carbonate hydrates ($\text{La}_2(\text{CO}_3)_3 \cdot 3.4\text{H}_2\text{O}$) with the orthorhombic type was synthesized by hydrothermal method. The thermal decomposition of $\text{La}_2(\text{CO}_3)_3 \cdot 3.4\text{H}_2\text{O}$ below 1,373 K was characterized by XRD, FTIR and DTA–TG. The nonisothermal decomposition kinetics of $\text{La}_2(\text{CO}_3)_3 \cdot 3.4\text{H}_2\text{O}$ over the temperature range of 360–566 °C was investigated by using NETZSCH Thermokinetics software.

Experimental

Synthesis of lanthanum carbonate hydrates

Lanthanum chloride solution was prepared by adding lanthanum chloride (25 g) to 0.1 L deionized water. Ammonium bicarbonate (316 g) was dissolved in 2 L deionized water. These solutions were filtered through a funnel and flask under vacuum, respectively. The ammonium bicarbonate solution was introduced into lanthanum chloride solution in 3–4 h under stirring. During the reaction, the pH value of the mixture solution was controlled within the range of 3–4. After the reaction completed, deionized water was added to the mixture solution and maintained at 298–308 K for 3–4 h. The products were filtered under vacuum, washed with deionized water repeatedly and then dried in oven.

Characterization of lanthanum carbonate hydrates

The conventional TG–DTA measurements were taken by using a Netzsch STA409PC simultaneous thermal analyzer at heating rates of 10 K min^{-1} from 303 to 1,273 K. In nonisothermal kinetic studies, initially the samples were heated at the rate of 10 K min^{-1} from 303 to 523 K followed by holding for 1 h to obtain pure anhydrous $\text{La}_2(\text{CO}_3)_3$ and then heated to 873 K at six different heating rates of 10, 15, 20, 25, 40 and 45 K min^{-1} , respectively. The operational characteristics of the TG–DTA system are sample mass: 12 mg, sample pan: alumina and atmosphere: air, flowing at 30 mL min^{-1} . Prior to experiments, temperature calibration was performed. The nonisothermal kinetic analysis was conducted with the help of NETZSCH Thermokinetic software, using the measured TG data. The residuals after thermal analysis tests were identified using X-ray diffraction (XRD) and Fourier transform infrared (FTIR) spectra.

The structure of as-prepared product and its residuals after thermal analysis tests were studied by X-ray diffractometer (Rigaku D/MAX-IIIc) equipped with Ni filter and generates a beam of CuK α radiation ($\lambda = 0.1546 \text{ nm}$). The operational settings for all the XRD scans are voltage: 40 kV, current: 30 mA, range: $5 < 2\theta < 70^\circ$ and scanning speed: 0.6° s^{-1} .

Fourier transform infrared spectra were recorded on a Bruker Tensor 27 spectrometer by using KBr pellets method in the wavenumbers range of $4,000\text{--}400 \text{ cm}^{-1}$.

Results and discussion

Thermal analysis

Figure 1 shows the TG–DTA–DTG curves of the as-prepared product at a heating rate of 10 K min^{-1} from 303 to

1,273 K in air. Four steps of mass loss are found according to the DTG–TG curves, and the corresponding data of mass loss (ML) are listed in Table 1. All steps are endothermic reaction.

The first step and the second step are from 303 to 475 K ($ML = 8.28\%$, $T_{\max} = 402.2$ K) and from 475 to 639 K ($ML = 4.04\%$, $T_{\max} = 524$ K), respectively, with an overall mass loss of 12.34 %, which is in good agreement with the theoretical mass loss of 12.32 % and can be attributed for a two-step 3.4 water molecules eliminated from $\text{La}_2(\text{CO}_3)_3 \cdot 3.4\text{H}_2\text{O}$. The first dehydration step involves the elimination of 2.3 mol H_2O from $\text{La}_2(\text{CO}_3)_3 \cdot 3.4\text{H}_2\text{O}$ and formation of $\text{La}_2(\text{CO}_3)_3 \cdot 1.1\text{H}_2\text{O}$, and the second dehydration step corresponds to the loss of the 1.1 remaining water molecules and formation of anhydrous $\text{La}_2(\text{CO}_3)_3$. The third step ($T = 639$ – 839 K, $ML = 16.74\%$, $T_{\max} = 790.1$ K) can be assigned to the decomposition of anhydrous $\text{La}_2(\text{CO}_3)_3$ and formation of dioxycarbonate, $\text{La}_2\text{O}_2\text{CO}_3$, since the experimental value of the mass loss for this step is close to the theoretical value (16.61 %).

However, from Fig. 1, it can be seen that no plateau appears in TG curve between 473 and 673 K, indicating that the dehydration reaction is not finished before the beginning of the decomposition of $\text{La}_2(\text{CO}_3)_3$. The authors try to obtain pure anhydrous $\text{La}_2(\text{CO}_3)_3$ by adding an isothermal segment at 523 K in the thermal decomposition process of $\text{La}_2(\text{CO}_3)_3 \cdot 3.4\text{H}_2\text{O}$. As temperature curve shown in Fig. 2, initially the samples were heated from 303 to 523 K at a rate of 10 K min^{-1} followed by holding for 1 h and then heated to 873 K at a rate of 10 K min^{-1} . The TG curve is shown in Fig. 2. It can be seen that as sample heated at 523 K for 30–60 min, the mass of the sample remained almost stable. The relative XRD patterns given in Fig. 3a show that the same amorphous phase assigned to anhydrous $\text{La}_2(\text{CO}_3)_3$ as a result of water loss. The

crystalline phase of anhydrous $\text{La}_2(\text{CO}_3)_3$ can only be produced from the lanthanite phase after drying the sample in a vacuum and then heated to 703 K in a 100 kPa CO_2 atmosphere [16]. From Fig. 3b, it can be found that the samples sintered at 853 K, and all diffraction peaks are indexed as well-crystallized $\text{La}_2\text{O}_2\text{CO}_3$ (PDF card 48-1113), indicating that Step 2 labeled in Fig. 2 assigned to the decomposition of anhydrous $\text{La}_2(\text{CO}_3)_3$ and formation of dioxycarbonate, $\text{La}_2\text{O}_2\text{CO}_3$. The total mass loss (29.06 %) of Step 1 and Step 2 obtained from Fig. 2 is similar to the total mass loss (29.02 %, 303–839 K) of the dehydration and the $\text{La}_2(\text{CO}_3)_3$ decomposition to $\text{La}_2\text{O}_2\text{CO}_3$ presented in Fig. 1 and Table 1. By comparing Figs. 1 and 2, it can be found that the mass of the overlapping step between the dehydration and the decomposition of $\text{La}_2(\text{CO}_3)_3$ shown in Fig. 1 is about 0.4 %, which assigned to the loss of the remaining water molecules, and can be released by adding an isothermal segment at 523 K for 1 h in the thermal decomposition of $\text{La}_2(\text{CO}_3)_3 \cdot 3.4\text{H}_2\text{O}$.

The fourth step ($T = 839$ – $1,123$ K, $T_{\max} = 1,065.3$ K), with a mass loss of 8.21 %, which is same as the theoretical mass loss of 8.31 %, accounts for the decomposition of $\text{La}_2\text{O}_2\text{CO}_3$ and formation of La_2O_3 . The thermal decomposition process of the as-prepared product is listed in Table 1 and evidentially confirmed by the results of XRD and IR experimental below.

XRD analysis

The XRD patterns of $\text{La}_2(\text{CO}_3)_3 \cdot 3.4\text{H}_2\text{O}$ and its residuals after thermal analysis tests are given in Fig. 4. From Fig. 4a, the result shows that all diffraction peaks of unheated sample are similar to those of the standard XRD patterns of the orthorhombic type of $\text{La}_2(\text{CO}_3)_3 \cdot 4\text{H}_2\text{O}$, with space group $\text{Pmp}21(18)$ and lattice constants $a = 9.57$, $b = 12.65$ and $c = 8.94 \text{ \AA}$, from PDF card 06-0076. The strong diffraction peak at 13.53° for 2θ is attributed to the layered structure of $\text{La}_2(\text{CO}_3)_3 \cdot 3.4\text{H}_2\text{O}$ [17]. No diffraction peaks of impurities are observed, which indicates that the single-phase $\text{La}_2(\text{CO}_3)_3 \cdot 3.4\text{H}_2\text{O}$ is synthesized.

From Fig. 4a, it can be found that the samples sintered at 403 K become poorly crystallized, while the characteristic diffraction peaks of the samples sintered between 441 and 633 K almost disappear except $2\theta = 18.4^\circ$, the products become amorphous [18]. The peak at $2\theta = 18.4^\circ$ corresponds to (020) plane in the orthorhombic structure [17]. The results indicate that the water of hydration is very important for the lanthanum carbonate hydrates. From Fig. 4b, it can be seen that both the phases of $\text{La}_2\text{O}(\text{CO}_3)_2$ and $\text{La}_2\text{O}_2\text{CO}_3$ exist in the samples sintered at 788 and 798 K, which are identified using PDF card 32-0490 and 48-1113, respectively. However, when the samples sintered at 813 and 853 K, the diffraction peaks of $\text{La}_2\text{O}(\text{CO}_3)_2$

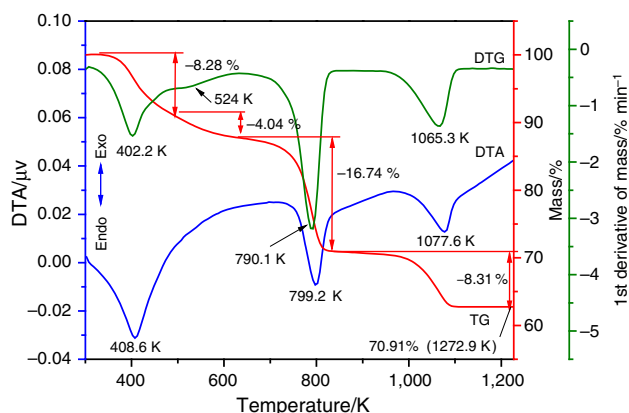
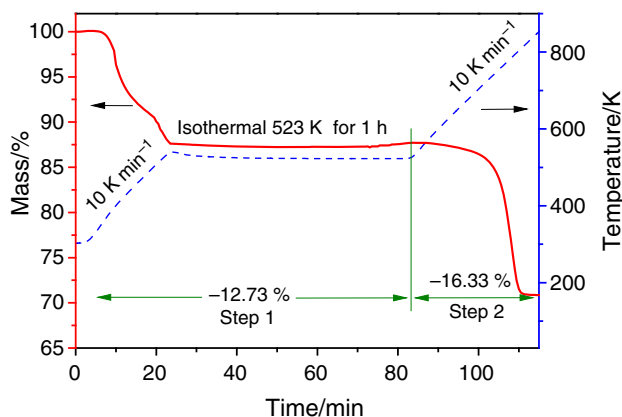


Fig. 1 DTA–TG–DTG curves of $\text{La}_2(\text{CO}_3)_3 \cdot 3.4\text{H}_2\text{O}$ at a heating rate of 10 K min^{-1} below 1,273 K in air

Table 1 Comparison of the experimental and theoretical mass loss values of $\text{La}_2(\text{CO}_3)_3 \cdot 3.4\text{H}_2\text{O}$

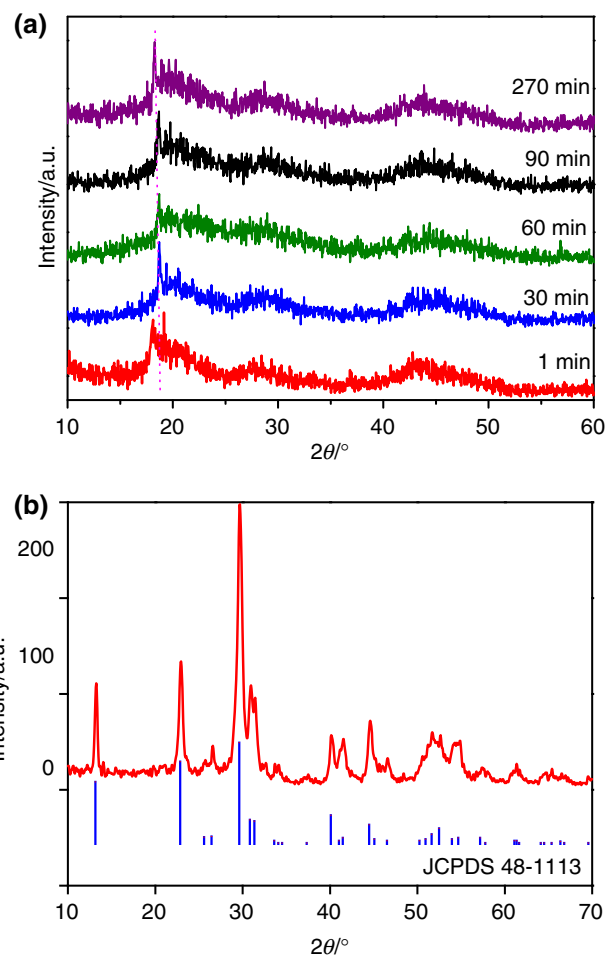
Stage	Temperature range/K	Mass loss/%		Solid residue
		Experimental	Theoretical	
1	303–475	−8.28	−8.33	$\text{La}_2(\text{CO}_3)_3 \cdot 1.1\text{H}_2\text{O}$
2	475–639	−4.04	−3.99	$\text{La}_2(\text{CO}_3)_3$
3	639–839	−16.74	−16.61	$\text{La}_2\text{O}_2\text{CO}_3$
4	839–1,123	−8.21	−8.31	La_2O_3

**Fig. 2** TG curve of sample heated to 523 K followed by holding for 1 h and then heated to 873 K at a heating rate of 10 K min^{-1}

disappear and those of $\text{La}_2\text{O}_2\text{CO}_3$ become sharper, indicating that the anhydrous $\text{La}_2(\text{CO}_3)_3$ is fully transformed to well-crystallized $\text{La}_2\text{O}_2\text{CO}_3$. This is consistent with conclusions reported in the literature using unconventional techniques that an additional intermediate product, $\text{La}_2\text{O}(\text{CO}_3)_2$, was formed in the decomposition of anhydrous $\text{La}_2(\text{CO}_3)_3$ to $\text{La}_2\text{O}_2\text{CO}_3$ [11, 12]. When the calcination temperature is increased to 1,078 K, all diffraction peaks detected of the products are indexed as well-crystallized La_2O_3 (PDF card 05-0602), indicating that the $\text{La}_2\text{O}_2\text{CO}_3$ is transformed to La_2O_3 .

IR spectroscopic analysis

The FTIR spectra of $\text{La}_2(\text{CO}_3)_3 \cdot 3.4\text{H}_2\text{O}$ and its residuals after thermal analysis tests are recorded in Fig. 5. The IR spectra of unheated $\text{La}_2(\text{CO}_3)_3 \cdot 3.4\text{H}_2\text{O}$ (Fig. 5a) show that the main bands at $3,464$ and $1,647 \text{ cm}^{-1}$ are due to lattice water vibration and the carbonate anion at $1,091 \text{ cm}^{-1}$ (symmetric stretching), $1,473$ and $1,357 \text{ cm}^{-1}$ (asymmetric stretching), 749 cm^{-1} (symmetric bend), 880 , 850 , 806 cm^{-1} (asymmetric bend) [17, 19]. The two main bands at 638 and 680 cm^{-1} are due to lattice vibration of $\text{La}-\text{O}$ [11]. The IR spectra characteristic peaks of unheated $\text{La}_2(\text{CO}_3)_3 \cdot 3.4\text{H}_2\text{O}$ showed at 850 , 749 , 680 cm^{-1} , respectively, are very close to $\text{La}_2(\text{CO}_3)_3 \cdot 3.3\text{H}_2\text{O}$ at 849 , 747 , 681 cm^{-1} [20], and rather than $\text{La}(\text{OH})\text{CO}_3$ at 858 ,

**Fig. 3** XRD patterns of sample heated at 523 K for different time duration (a) and their calcination products at 853 K (b)

724 , 696 cm^{-1} [20]. These results indicate to not contain impurities such as $\text{La}(\text{OH})\text{CO}_3$ in the as-prepared products, which as an undesirable by-product is easily formed during the preparation of dehydrated lanthanum carbonates [20]. Although it has been published that $\text{La}(\text{OH})\text{CO}_3$ can also bind phosphate [21], it is not clear whether the $\text{La}(\text{OH})\text{CO}_3$ is safe in medical application [20].

The IR spectrum of the sample sintered at 403 K shows that the lattice water vibration at $1,647 \text{ cm}^{-1}$ has weakened and totally disappeared at 633 K (Fig. 5b), which reveal that the

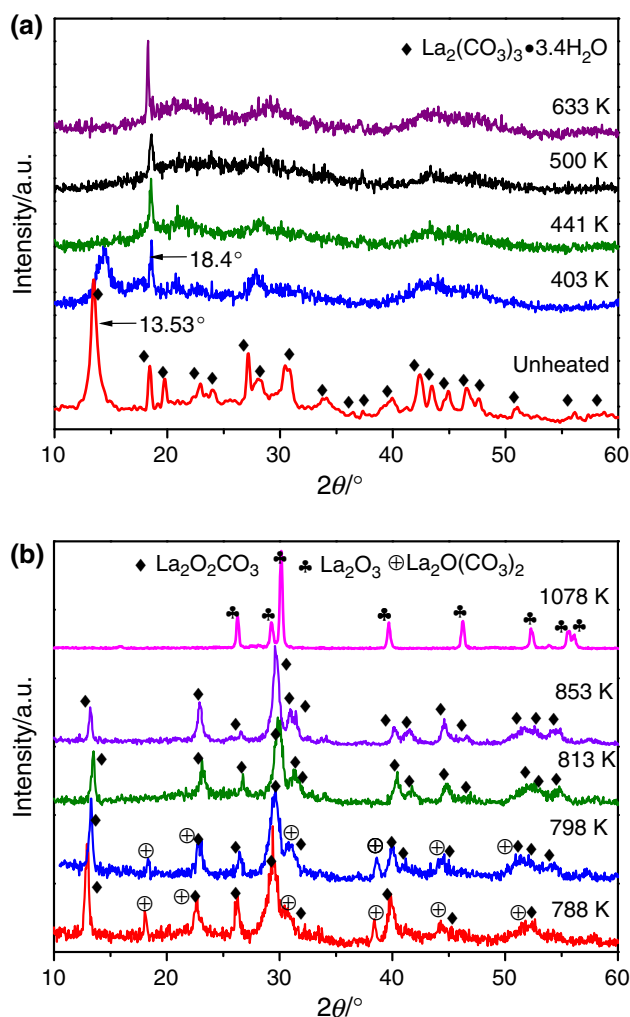


Fig. 4 XRD patterns for the as-prepared $\text{La}_2(\text{CO}_3)_3 \cdot 3.4\text{H}_2\text{O}$ and its calcination products at 403–633 K (a), 788–1,078 K (b)

dehydration reaction finishes in this range. While the absorptive peaks between $1,000$ and 600 cm^{-1} assignable to CO_3^{2-} species distinctly become strong between 403 and 633 K, the absorptions band at $2,345\text{ cm}^{-1}$ begins to appear as a result of water loss [17]. The IR spectrum of the sample sintered at 853 K (Fig. 5b) shows strong absorption between 1600 and $1,300\text{ cm}^{-1}$ and also at 1,060 and 870 cm^{-1} assignable to oxycarbonate species as a result of the formation of $\text{La}_2\text{O}(\text{CO}_3)_2$ and $\text{La}_2\text{O}_2\text{CO}_3$ [19]. The FTIR spectra of the sample sintered 1,078 K (Fig. 5b) show that the characteristic absorbance band at about 650 cm^{-1} is related to lattice vibration modes of La_2O_3 [11], whereas the weak bands around $3,610$, $1,600$ and $1,500\text{ cm}^{-1}$ are most probably due to surface contamination by carbonate and moisture [12]. These are consistent with the results of TG–DTG, DTA and XRD experimental.

The combination of XRD, FTIR, TG–DTA analysis techniques allows to suggest the thermal process of $\text{La}_2(\text{CO}_3)_3 \cdot 3.4\text{H}_2\text{O}$ as following four steps:

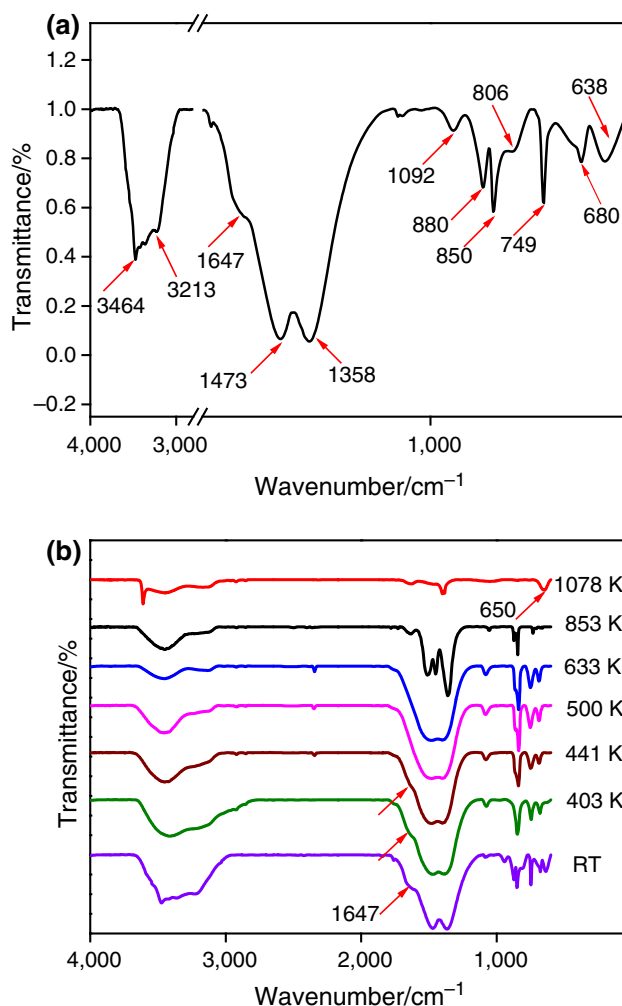
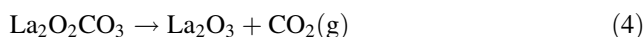
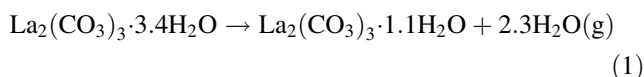


Fig. 5 IR spectra for as-prepared $\text{La}_2(\text{CO}_3)_3 \cdot 3.4\text{H}_2\text{O}$ (a) and its calcination products at RT–1,078 K (b)



Nonisothermal kinetics

The aim of nonisothermal kinetic studies is the investigation of the decomposition mechanism of anhydrous $\text{La}_2(\text{CO}_3)_3$ to $\text{La}_2\text{O}_2\text{CO}_3$. Accordingly, initially the samples were heated at a rate of 10 K min^{-1} from 303 to 523 K followed by holding for 1 h to obtain pure anhydrous $\text{La}_2(\text{CO}_3)_3$ and then heated to 873 K at six different heating rates of 10, 15, 20, 25, 40 and 45 K min^{-1} , respectively.

Figure 6 shows TG and DTG curves of the samples after isothermal and then heated at six different heating rates. It can be seen that under different heating rates similar TG curves are obtained, and the mass loss is independent of the heating rate. However, with increasing rates of heating, there is difference on the DTG curves: DTG curves under heating rate 10, 15, 20 and 25 K min⁻¹ show only one peak, whereas DTG curves under heating rate 40 and 45 K min⁻¹ show a strong peak and an additional shoulder, respectively. For its description, the reaction can be divided into two stages, and the intermediate stage can be kinetically hindered one. This is consistent with results of XRD analysis and conclusions reported by Balboul [11] and Vanhoyland [12].

Estimation of the activation energy E

The kinetic equation of thermal decomposition can be expressed by Eq. (5) [22]

$$\frac{d\alpha}{dT} = \frac{A}{\beta} \exp[-E/(RT)]f(\alpha) \quad (5)$$

where T is the temperature, α is the extent of conversion, β is the linear heating rate, $f(\alpha)$ is the reaction mechanism function, A is the pre-exponential factor, E is the apparent activation energy, R is the gas constant. The purpose of this paper is to obtain the three factors of the above equations, i.e., E , A and $f(\alpha)$ by using the following FWO and FRL methods.

Flynn–Wall–Ozawa (FWO) Method

Equation (6) is FWO method, which follows from logarithmic form of Eq. (5) [23].

$$\ln \beta = \log \left[\frac{AE}{Rf(\alpha)} \right] - 2.315 - 0.456 \frac{E}{RT} \quad (6)$$

In terms of the FWO method equation, the slope of $\ln \beta$ versus $1/T$ for the same value of α gives the value of E , and A can be calculated by intercept when $f(\alpha)$ is coincident.

Friedman–Reich–Levi (FRL) Method

By integration of Eq. (5), the following FRL method Eq. (7) is obtained [24].

$$\ln \left(\frac{\beta d\alpha}{dT} \right) = \ln [Af(\alpha)] - \frac{E}{RT} \quad (7)$$

Based on the FRL method equation, the slope of $\ln [\beta(d\alpha/dT)]$ versus $1/T$ for the same value of α gives the value of E , and A can be calculated by intercept when $f(\alpha)$ is coincident. It can give information about reaction mechanisms that can occur in more than one step.

The E and A can be calculated from the slopes of the $\ln [\beta(d\alpha/dT)]$ versus $1/T$ and $\ln \beta$ versus $1/T$ based on the FRL and FWO method equation, respectively. The E values calculated using the FWO and FRL methods based on the TG data (10, 15, 20, 25 K min⁻¹) below 873 K are shown in Fig. 7. It can be seen that both FRL and FWO isoconversional methods give consistent values of E with good correlation, so that the results are credible. However, the FRL methods analysis produces a higher error bars in the energy plot rather than the FWO methods. It was considered that the E values are independent of α if the relative error of the slope of the FWO equation straight line is lower than 10%. If E value is independent of α , the decomposition may be a simple reaction; otherwise, it is a multistep reaction mechanism [25]. According to the characteristics of the E - α plot of using the FWO methods, the activation energies are 435 kJ mol⁻¹ at beginning and, with increasing mass loss, it drops sharply to 260 kJ mol⁻¹, then reach a plateau or constant with mean

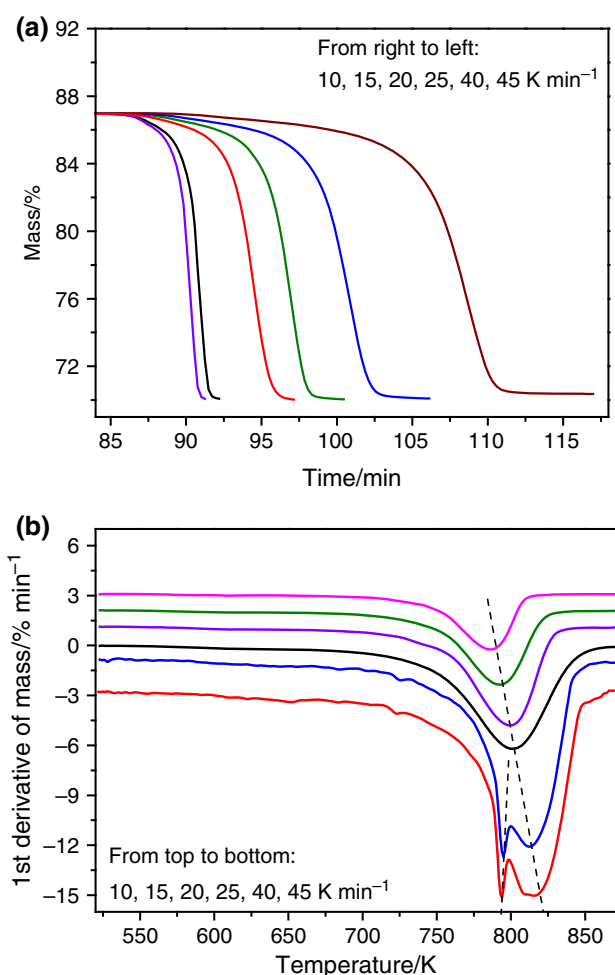


Fig. 6 TG (a) and DTG (b) curves of $\text{La}_2(\text{CO}_3)_3 \cdot 3.4\text{H}_2\text{O}$ under different heating rates

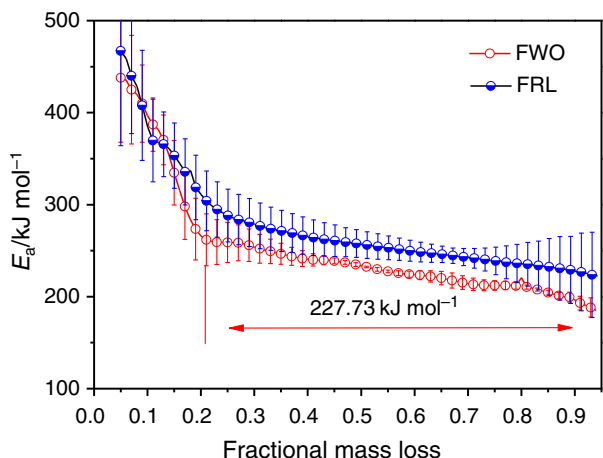


Fig. 7 Activation energies as a function of conversion degree by FRL, FWO methods

value of $E = 227.73 \text{ kJ mol}^{-1}$, indicating that the reaction proceeds with two stages [26].

Determination of the most probable mechanism

According to the results of FWO and FRL method analysis, multivariate nonlinear regression (NETZSCH Thermokinetics) was applied to determinate the most probable kinetic model combined with 23 conversion functions [27]. The activation energies calculated with FWO method act as initial values for multivariate nonlinear regression process. The quality of the best fitting was determined with the use of value F_{exp} [22] and regression coefficient. The following schemes (mechanisms) of process were also considered: scheme coded by d:f (consecutive path), d:c (competitive path) and d:p (parallel path).

Based on the results listed in Table 2 tested by multivariate nonlinear regression, the best-fit quality was obtained for the schemes coded by d:f with the conversion functions F_n-F_n and A_n-A_n , respectively, with the highest correlation coefficient (0.99835), and the F_{exp} value not exceeding the critical value (F_{crit}) [27]. The corresponding kinetic parameters are listed in Table 3. From Table 3, it can be found that the E values matching with the two-stage consecutive mechanism with the conversion functions A_n-A_n are close to the values obtained by FWO methods. This is considered enough to conclude that the best model was obtained for the two-stage consecutive mechanism (A_n-A_n), and the kinetic parameters of nonisothermal decomposition are reliably calculated with the most probable kinetic model.

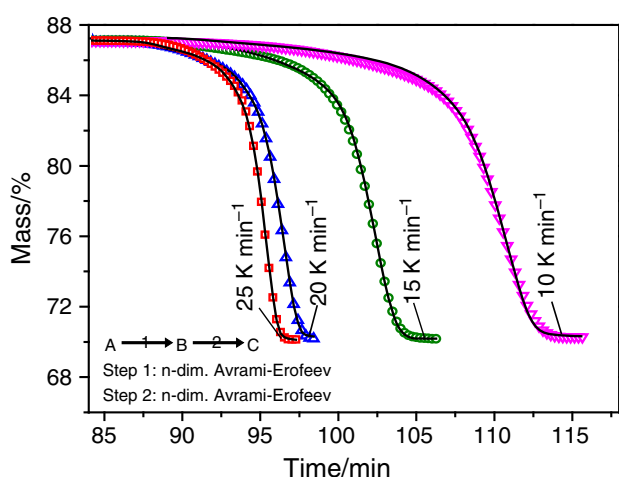
The plots of multivariate nonlinear regression with the best model are presented in Fig. 8. It is seen that there are a good agreement between all the experimental and fitted TG curves. According to Table 3, the thermal decomposition of anhydrous $\text{La}_2(\text{CO}_3)_3$ to $\text{La}_2\text{O}_2\text{CO}_3$ is controlled by two-stage consecutive mechanism, an n -dimensional growth of nuclei (Avrami equation) initial reaction followed by n -dimensional growth of nuclei consecutive reaction, and the corresponding function is $f(\alpha) = n(\ln(1 - \alpha^{(1 - 1/n)})) (1 - \alpha)$. The first stage: $E = 435 \pm 8 \text{ kJ mol}^{-1}$, $\lg A = 28.7 \pm 0.8$, $\text{Dimension1} = 0.28$; the second stage: $E = 234 \pm 4 \text{ kJ mol}^{-1}$, $\lg A = 13.5 \pm 0.3$, $\text{Dimension2} = 1.22$. These forms of the Avrami equation (parameter $m = 0.28$ and 1.22) denote a small and large contribution of diffusion to the two-stage process [28], respectively. We estimated the contribution of each stage: The first stage is 20.5 %, and the second stage reaction is 79.5 % of the decomposition (Table 2).

Table 2 Results of F test on fit quality of different model obtained by nonlinear regression

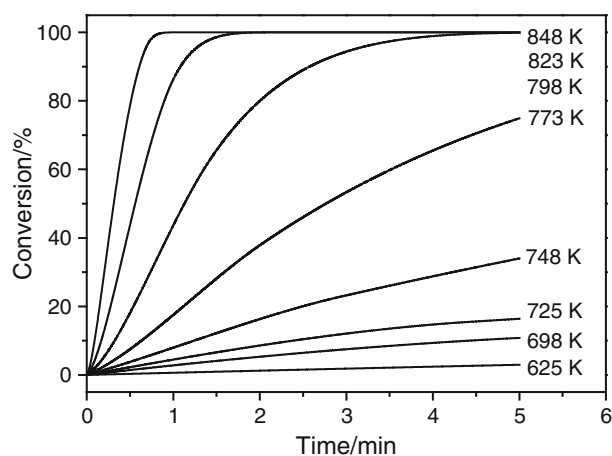
No.	Code	Scheme	F_{exp}	F_{crit}	Correlation coefficient	Type 1	Type 2	Contribution of step/%	
								First	Second
1	d:f	A $\xrightarrow{1}$ B $\xrightarrow{2}$ C	1.00	1.17	0.99835	A_n	A_n	20.52	79.48
2	d:f	A $\xrightarrow{1}$ B $\xrightarrow{2}$ C	1.00	1.17	0.99835	F_n	F_n	14.85	75.15
3	d:c	A $\xrightarrow{1}$ B $\xrightarrow{2}$ C	1.29	1.17	0.99829	A_n	F_n	95.68	4.32
4	d:f	A $\xrightarrow{1}$ B $\xrightarrow{2}$ C	1.31	1.17	0.9940	A_n	F_n	16.06	83.94
5	d:f	A $\xrightarrow{1}$ B $\xrightarrow{2}$ C	1.39	1.17	0.99389	F_n	A_n	16.48	83.52
6	d:c	A $\xrightarrow{1}$ B $\xrightarrow{2}$ C	1.74	1.17	0.99764	A_n	A_n	54.17	45.83
7	d:c	A $\xrightarrow{1}$ B $\xrightarrow{2}$ C	4.08	1.17	0.99454	F_n	F_n	1.19	98.81
8	d:f	A $\xrightarrow{1}$ B $\xrightarrow{2}$ C	5.88	1.17	0.99199	R_2	R_2	8.41	91.59
9	d:f	A $\xrightarrow{1}$ B $\xrightarrow{2}$ C	10.16	1.17	0.98627	D_2	D_2	31.05	68.95
10	d:c	A $\xrightarrow{1}$ B $\xrightarrow{2}$ C	51.4	1.17	0.95567	F_n	A_n	99.64	0.36

Table 3 Nonisothermal kinetic and statistic parameters after nonlinear regression through the two-stage model d:f

Stage	Function	$f(\alpha)$	$E/\text{kJ mol}^{-1}$	$\log A/\text{s}^{-1}$	Kinetic parameter	Reaction parameter	Fit quality
1st	A_n	$n(\ln(1 - \alpha^{(1-1/n)})) / (1 - \alpha)$	435 ± 9	28.7 ± 0.8	$\text{Dimension1} = 0.28$	$\text{Foll. React. } l = 0.22$	Correlation coefficient: 0.99835, $t\text{-valalpha} = 0.95,492: 1.95638,$
2nd	A_n		234 ± 4	13.5 ± 0.3	$\text{Dimension2} = 1.22$		Durbin–Watson factor: 2.34289
1st	F_n	$(1 - \alpha^n)$	89 ± 11	4.4 ± 0.8	$n = 1.24$	$\text{Foll. React. } l = 0.15$	Correlation coefficient: 0.99835, $t\text{-valalpha} = 0.95,492: 1.95638,$
2nd	F_n		227 ± 5	13 ± 0.3	$n = 0.82$		Durbin–Watson factor: 2.18363

**Fig. 8** Multivariate nonlinear regression results through two-step method d:f (the solid line is fitted values, and symbols are the experiment values)

Balboul [11] carried out a nonisothermal thermal decomposition kinetics study of lanthanum oxalate dehydrate. They showed that anhydrous $\text{La}_2(\text{CO}_3)_3$ was transformed into $\text{La}_2\text{O}(\text{CO}_3)_2$ and $\text{La}_2\text{O}_2\text{CO}_3$ at 698 and 743 K, and the corresponding reaction activation energies were 123 and 145 kJ mol^{-1} , respectively, but none provided the reaction model. The E value determined in the present study is significantly higher than the obtained one by Balboul [11], and the activation energy of the first reaction stage is significantly more than that of the second stage (434.9 and 234.3 kJ mol^{-1}). These are consistent with thermodynamic rule. Since $\text{La}_2\text{O}(\text{CO}_3)_2$ belongs to a metastable state phase, which are more easily transformed into steady $\text{La}_2\text{O}_2\text{CO}_3$ [29], that would mean lower energy is needed for the second step reaction, so that the results obtained in the present study are credible. Based on the Ref. [27], for the two-stage consecutive reaction, if the E values of the first stage are higher than that of the second stage, with increasing rates of heating, the separation of two peaks will become greater. Taking this into account,

**Fig. 9** Total mass loss under isothermal condition of $\text{La}_2(\text{CO}_3)_3 \cdot 3.4\text{H}_2\text{O}$ at temperature between 625 and 848 K

the appearance of one additional shoulder from the DTG curves under higher heating rates (40, 45 K min^{-1}) (Fig. 6b) can be explained.

The NETZSCH Thermokinetic software was also used to predict total mass loss and phase composition of $\text{La}_2(\text{CO}_3)_3 \cdot 3.4\text{H}_2\text{O}$ heated between 625 and 848 K under isothermal condition with the best model. The simulated results of total mass loss are shown in Fig. 9. This diagram represents, the decomposition is quickly completed for a time range of 0.8–5 min between 798 and 848 K. The prediction of product concentration of $\text{La}_2(\text{CO}_3)_3 \cdot 3.4\text{H}_2\text{O}$ heated at 798 K for 5 min is reported in Fig. 10. According to the results obtained by XRD measurements (Fig. 4b), it is concluded that phase A labeled in the diagram is $\text{La}_2(\text{CO}_3)_3$; phase B is $\text{La}_2\text{O}(\text{CO}_3)_2$; phase C is $\text{La}_2\text{O}_2\text{CO}_3$. As can be seen from Fig. 10, $\text{La}_2(\text{CO}_3)_3$ is quickly consumed. $\text{La}_2\text{O}(\text{CO}_3)_2$ begins to emerge as soon as $\text{La}_2(\text{CO}_3)_3$ began to decompose. The concentration of $\text{La}_2\text{O}(\text{CO}_3)_2$ reaches to the highest value after 1 min of reaction beginning and then decrease to zero up to 4 min. These results confirm that $\text{La}_2\text{O}(\text{CO}_3)_2$ is thermodynamically

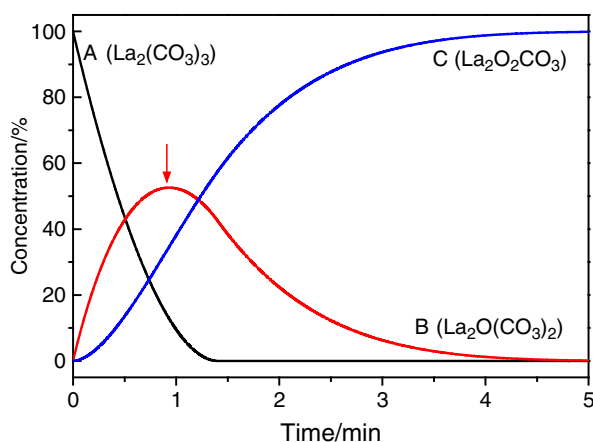


Fig. 10 Concentration of products for the isothermal reaction of $\text{La}_2(\text{CO}_3)_3 \cdot 3.4\text{H}_2\text{O}$ at 798 K

unstable in the process. As a result, the decomposition process of $\text{La}_2\text{O}(\text{CO}_3)_2$ has no inflection on TG curves. The possibility of such decomposition features, e.g., was showed by Logvinenko for the multistage dehydration of gadolinium hydroxide [30].

Conclusions

- (1) The single-phase $\text{La}_2(\text{CO}_3)_3 \cdot 3.4\text{H}_2\text{O}$ with the orthorhombic type was successfully prepared by hydrothermal method. The thermal decomposition process of $\text{La}_2(\text{CO}_3)_3 \cdot 3.4\text{H}_2\text{O}$ below 1,273 K involves four steps: a two-step dehydration and formation of anhydrous $\text{La}_2(\text{CO}_3)_3$ at first, and then the formation of $\text{La}_2\text{O}_2\text{CO}_3$ and La_2O_3 , respectively.
- (2) Thermal decomposition of $\text{La}_2(\text{CO}_3)_3$ to $\text{La}_2\text{O}_2\text{CO}_3$ can be divided into two stages based on the DTG curves under higher heating rates (40, 45 K min^{-1}). An additional intermediate stage assigned to the formation of $\text{La}_2\text{O}(\text{CO}_3)_2$ was observed in the thermal decomposition of $\text{La}_2(\text{CO}_3)_3$ to $\text{La}_2\text{O}_2\text{CO}_3$. The activation energies calculated by FWO and FRL isoconversional methods also confirm that the reaction is not a simple process.
- (3) Thermal decompositions of $\text{La}_2(\text{CO}_3)_3$ to $\text{La}_2\text{O}_2\text{CO}_3$ are controlled by a kind of two-stage consecutive reaction (A_n-A_n model), an n -dimensional growth of nuclei (Avrami equation) initial reaction followed by n -dimensional growth of nuclei consecutive reaction, $f(\alpha) = n(\ln(1 - \alpha^{(1 - 1/n)})(1 - \alpha))$. The first stage: $E = 435 \pm 9 \text{ kJ mol}^{-1}$, $\lg A = 28.7 \pm 0.8$, $\text{Dimension}1 = 0.28$; the second stage: $E = 234 \pm 4 \text{ kJ mol}^{-1}$, $\lg A = 13.5 \pm 0.3$, $\text{Dimension}2 = 1.22$.

Acknowledgements The authors would like to thank Mrs. Jing Liu and Mr. Miao Deng for their contribution to the FTIR and XRD measurements, and Mr. Liang Xu from NETZSCH Scientific Instrument Trading Co., LTD., Shanghai Branch, for his helpful discussions. This study was financed by The National Land and Resources Public Welfare Scientific Research Project of China (201011005-5), National Natural Science Foundation of China (50974025), Specialized Research Fund for the Doctoral Program of Higher Education of China (20095122110015), Key Project of National Natural Science Foundation of China (41030426), Key Project of Extracurricular Scientific Research for the University Student of Chengdu University of Technology (2014KL148) and Scientific Research Foundation of the Education Ministry for Returned Chinese Scholars, China (2010-32).

References

1. Moerck R, Prochazka J, Schauer E, Spitler T. Rare earth metal compounds methods of making, and methods of using the same. Google Patents; 2011.
2. Albaaj F, Hutchison A. Lanthanum carbonate (Fosrenol®): a novel agent for the treatment of hyperphosphataemia in renal failure and dialysis patients. *Int J Clin Pract.* 2005;59:1091–6.
3. Vadivel Murugan A, Navale S, Ravi V. Synthesis of nanocrystalline La_2O_3 powder at 100°C. *Mater Lett.* 2006;60:848–9.
4. Petryk J, Kotakowska E. Cobalt oxide catalysts for ammonia oxidation activated with cerium and lanthanum. *Appl Catal B.* 2000;24:121–8.
5. Escudero M, Novoa X, Rodrigo T, Daza L. Influence of lanthanum oxide as quality promoter on cathodes for MCFC. *J Power Sources.* 2002;106:196–210.
6. Schweizer T, Samson B, Hector J, Brocklesby W, Hewak D, Payne D. Infrared emission from holmium doped gallium lanthanum sulphide glass. *Infrared Phys Technol.* 1999;40:329–37.
7. Zhang KL, Chen XB, Xi MY, Song L, Zhang XF, Sun JT. Thermal decomposition of lanthanum oxalate decahydrate. *J Wuhan U-Nat.* 1996;42:163–6.
8. Panchula ML, Akinc M. Morphology of lanthanum carbonate particles prepared by homogeneous precipitation. *J Eur Ceram Soc.* 1996;16:833–9.
9. Bates S, Hallenbeck D. Method for use of lanthanum carbonate pharmaceutical compositions. Google Patents; 2009.
10. Salavati-Niasari M, Mir N, Davar F. A novel precursor in preparation and characterization of nickel oxide nanoparticles via thermal decomposition approach. *J Alloys Compd.* 2010;493:163–8.
11. Balboul BAA, Roudi AEL, Samir E, Othman A. Non-isothermal studies of the decomposition course of lanthanum oxalate decahydrate. *Thermochim Acta.* 2002;387:109–14.
12. Vanhoyland G, Nouwen R, Van Bael M, Yperman J, Mullens J, Van Poucke L. The use of Hi-Res TGA, TG-FTIR, HT-DRIFT and HT-XRD in the study of the decomposition of $\text{La}_2(\text{C}_2\text{O}_4)_3 \cdot \text{H}_2\text{O}$. *Thermochim Acta.* 2000;354:145–51.
13. Logvinenko V, Bakovets V, Trushnikova L. Decomposition processes of nickel hydroxide. *J Therm Anal Calorim.* 2012;107:983–5.
14. Machuron-Mandard XR, Madic C. Plutonium dioxide particle properties as a function of calcination temperature. *J Alloys Compd.* 1996;235:216–8.
15. Celis K, Driessche VI, Mouton R, Vanhoyland G, Hoste S. Kinetics of consecutive reactions in the solid state: thermal decomposition of oxalates. *Meas Sci Rev.* 2001;1:177–80.

16. Leskela M, Niinisto L. Handbook on the physics and chemistry of rare earths. Amsterdam: Elsevier; 1986.
17. Brown ME, Dollimore D, Galwey AK. Reactions in the solid state. Amsterdam: Elsevier; 1980.
18. Redfern SA. Structural variations in carbonates. *Rev Miner Geochem.* 2000;41(1):289–310.
19. Nakamoto K. Infrared and Raman spectra of inorganic and coordination compounds. Part B., Applications in coordination, organometallic, and bioinorganic chemistry. London: Wiley; 2009.
20. He A, Zhou F, Ye F, Zhang Y, He X, Zhang X, et al. Preparation and characterization of lanthanum carbonate octahydrate for the treatment of hyperphosphatemia. *J Spectrosc.* 2013. doi:[10.1155/2013/593636](https://doi.org/10.1155/2013/593636).
21. Muddasani PR, Talasila SR, Satya ERAK, Satti VR, Nannapaneni VC. Process for the preparation of lanthanum carbonate dihydrate. Google Patents; 2012.
22. Vlaev LT, Nikolova MM, Gospodinov GG. Non-isothermal kinetics of dehydration of some selenite hexahydrates. *J Solid State Chem.* 2004;177:2663–9.
23. Flynn J. A general differential technique for the determination of parameters for $d(\alpha)/dt = f(\alpha) A \exp(-E/RT)$. *J Therm Anal Calorim.* 1991;37:293–313.
24. Opfermann J, Blumm J, Emmerich W-D. Simulation of the sintering behavior of a ceramic green body using advanced thermokinetic analysis. *Thermochim Acta.* 1998;318:213–8.
25. Mocioiu OC, Zaharescu M, Jitianu G, Budrugaec P. Kinetic parameters determination in non-isothermal conditions for the crystallisation of a silica-soda-lead glass. *J Therm Anal Calorim.* 2006;86:429–36.
26. Mothé MG, Carvalho CH, Sérvulo EF, Mothé CG. Kinetic study of heavy crude oils by thermal analysis. *J Therm Anal Calorim.* 2013;111:663–8.
27. Opfermann J. Manual of the Program NETZSCH Thermokinetics. Version; 1998.
28. Logvinenko V, Belyaev AV, Vorobeva SN. Dehydration process of rhodium sulfate crystalline hydrate. *J Therm Anal Calorim.* 2013. doi:[10.1007/s10973-013-3083-6](https://doi.org/10.1007/s10973-013-3083-6).
29. Shirsat A, Ali M, Kaimal K, Bharadwaj S, Das D. Thermochemistry of $\text{La}_2\text{O}_2\text{CO}_3$ decomposition. *Thermochim Acta.* 2003;399:167–70.
30. Logvinenko V, Bakovets V, Trushnikova L. Dehydroxylation kinetics of gadolinium hydroxide. *J Therm Anal Calorim.* 2014;115:517–21.